Author(s): Majumdar, Sayani & van Dijken, Sebastiaan

Title: Pulsed laser deposition of La1-xSrxMnO3 : thin-film properties and spintronic applications

Year: 2013

Version: Post print

Please cite the original version:

Majumdar, Sayani & van Dijken, Sebastiaan. 2013. Pulsed laser deposition of La1-xSrxMnO3 : thin-film properties and spintronic applications. Journal of Physics D: Applied Physics. Volume 47, Issue 3. 034010/1-15. ISSN 0022-3727 (printed). DOI: 10.1088/0022-3727/47/3/034010

Pulsed laser deposition of $La_{1-x}Sr_xMnO_3$: Thin film properties and spintronic applications

Sayani Majumdar[1,2] and Sebastiaan van Dijken[1]

[1]NanoSpin, Department of Applied Physics, Aalto University School of Science, P.O. Box 15100, FI-00076 Aalto, Finland

[2]Wihuri Physical Laboratory, Department of Physics and Astronomy, University of Turku, FI-20014 Turku, Finland

Abstract

Materials engineering at the nanoscale by precise control of growth parameters can lead to many unusual and fascinating physical properties. The development of pulsed laser deposition (PLD) 25 years ago has enabled atomistic control of thin films and interfaces and as such it has contributed significantly to advances in fundamental material science. One application area is the research field of spintronics, which requires optimized nanomaterials for the generation and transport of spin-polarized carriers. The mixed valence manganite $La_{1-x}Sr_xMnO_3$ (LSMO) is an interesting material for spintronics due to its intrinsic magnetoresistance properties, electric-field tunable metal-insulator transitions, and half-metallic band structure. Studies on LSMO thin-film growth by PLD show that the deposition temperature, oxygen pressure, laser fluence, strain due to substrate-film lattice mismatch, and post-deposition annealing greatly influence the magnetic and electrical transport properties of LSMO. For spintronic structures, robust ferromagnetic exchange interactions and metallic conductivity are desirable properties. In this article, we review the physics of LSMO thin films and the important role that PLD played to advance the field of LSMO-based spintronics. Some specific application areas including magnetic tunnel junctions (MTJs), multiferroic tunnel junctions (MFTJs), and organic spintronic devices are highlighted, and the advantages, drawbacks, and opportunities of PLD-grown LSMO for next-generation spintronic devices are discussed.

2. Introduction

The technology of spintronics uses the charge and spin of electrons to store information or to carry out logic operations [1, 2]. Spintronic components are often more versatile, energy efficient and faster than their conventional counterparts. Major developments in spintronics include giant magnetoresistance (GMR) [3] in metallic multi-layers and spin valve devices and tunneling magnetoresistance (TMR) [4] in MTJs. Both effects have been used in commercial applications including magnetic field sensors, the read head of magnetic hard-disk drives, and non-volatile magnetic random access memory (MRAM). Many functional spintronic devices require a highly spin-polarized injector and detector. $La_{1-x}Sr_xMnO_3$ (LSMO) with

x = 0.2 – 0.4 has been a popular choice as magnetic electrode in both inorganic and organic spin-based structures because of its fully spin polarized conduction band at the Fermi level [6]. Other interesting properties of LSMO include a matching work function with several organic semiconductors and polymers and a metal-insulator transition that is tunable by lattice strain and electric fields.

Pulsed laser deposition (PLD) [7] is a versatile thin-film deposition technique that can be used for nanoscale engineering of complex materials and interfaces. In correlated electron systems like LSMO, strong lattice-charge-spin coupling offers extensive control of magnetic and electronic transport properties by growth optimization and external actuation [8]. Besides intrinsic material parameters, spintronic elements often rely on band-structure effects at the interfaces between magnetic and non-magnetic thin films. Since the interface of LSMO is sensitive to bonding with other materials, charge transport due to polar discontinuities, and electric-field effects, it allows for the engineering of improved material responses and new functionalities. In this article, we review the use of PLD-grown LSMO films in spintronics. After an introduction to LSMO and a discussion on the control of LSMO properties using PLD, examples of LSMO films in MTJs, MFTJs, and organic spintronic devices are given.

3. $La_{1-x}Sr_xMnO_3$: Structural, magnetic and transport properties

Perovskite manganites with the general formula $R_{1-x}A_xMnO_3$ (where R = rare-earth cation and A = alkali or alkaline earth ion) have been widely investigated since the 1990s because of their interesting magnetic and electrical properties, such as colossal magnetoresistance (CMR) and composition- and temperature-dependent metal-insulator transitions. Among perovskite manganites, LSMO is an optimal choice for spintronic applications as it combines high carrier spin polarization, the highest Curie temperature ($T_C \approx 360$ K in thin films) within the manganites family [8], and low carrier density (10^{21} - 10^{22} cm^{-3}) [9]. Figure 1 illustrates the crystal structure of the LSMO unit cell. The lattice is approximated by a face-centered-cubic (fcc) structure with a Mn ion in the center and La/Sr cations at the corners of the cubic unit cell. Six oxygen ions surround the Mn ion and together they form a MnO_6 octahedron. For a perfect size match between the La and dopant cations, the tolerance factor $d_{A\text{-}O}/\sqrt{2}d_{Mn\text{-}O} = 1$ and the Mn-O-Mn bond angle is 180°. However, due to a mismatch between the radii of the cations, the unit cell of manganites becomes distorted with a modified MnO_6 octahedron. For hole doped LSMO with $x = 1/3$ and an average A-site radius of $\langle r_A \rangle \approx 1.24$ Å, the Mn-O-Mn bond angle is 166.3°. LSMO has a rhombohedral crystal structure with $R\ \bar{3}c$ space group symmetry [11]. The structural stability of LSMO is determined by charge neutrality, which also depends on the radius of the A-site dopant (Sr). In the LSMO lattice, the rare-earth La^{3+} ions are the largest, while the smaller Mn ions exhibit the mixed-valence phase of Mn^{3+} and Mn^{4+}, depending on the hole doping concentration x.

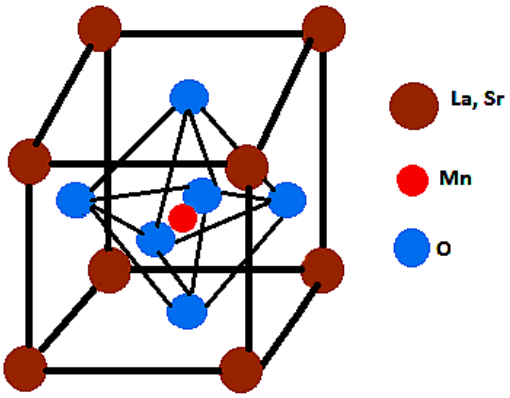

Figure 1. Schematic illustration of the LSMO crystal structure.

The electronic properties of LSMO are strongly correlated with the crystal structure. In an ideal perovskite structure, the five *d* orbitals of an isolated Mn ion undergo a crystal field splitting into a t_{2g} triplet (consisting of the d_{xy}, d_{xz} and d_{yz} orbitals) and an e_g doublet (originating from the $d_{x^2-y^2}$ and $d_{3z^2-r^2}$ orbitals) as schematically shown in Figure 2. The degeneracy of the levels is further lifted by lattice distortions that lower the crystal symmetry, also known as Jahn-Teller (*JT*) distortions. Due to the tetrahedral Mn-O coordination the t_{2g} triplet is energetically lower than the e_g doublet. Lifting of the two-fold degeneracy of the e_g spin-up and spin-down bands by *JT* distortions results in the spin-resolved band structure of LSMO [6]. Therefore, in the Mn^{4+} valence states the low-lying t_{2g} states are occupied by three parallel-spin electrons forming a $S = 3/2$ core spin while in the Mn^{3+} valence state ($S = 2$) the additional electron occupies a higher-lying e_g state (with crystal field splitting $\Delta \approx 1.5$ eV between the lowest t_{2g} and the highest e_g level). As substitution of each trivalent La^{3+} by divalent Sr^{2+} in $LaMnO_3$ induces itinerant holes, a doping concentration of $x = 0.3 - 0.4$ leads to a roughly equal number of Mn^{3+} and Mn^{4+}. Depending on doping concentration, LSMO has a conduction band that is either more ($x < 0.5$) or less ($x > 0.5$) than half-filled. In hole-doped LSMO ($x < 0.5$), the fully occupied spin-up localized t_{2g} band and partially occupied spin-up e_g band are separated from the empty minority bands by a large Hund's energy of about 2.5 eV. For both spin orientations, the oxygen 2*p* states are fully occupied and the electronic structure near the Fermi level is determined by hybridization between the majority spin Mn-e_g states and the O-*p* states. The minority spin states and the O-2*p* band are separated by an insulating band gap and therefore only majority carriers are present at the Fermi level, i.e. LSMO is a half metal for $x = 0.3 - 0.4$. The 100% spin polarization at the Fermi level of LSMO is much larger compared to the ≈40% spin polarization of ferromagnetic 3*d* transition metals [11-14].

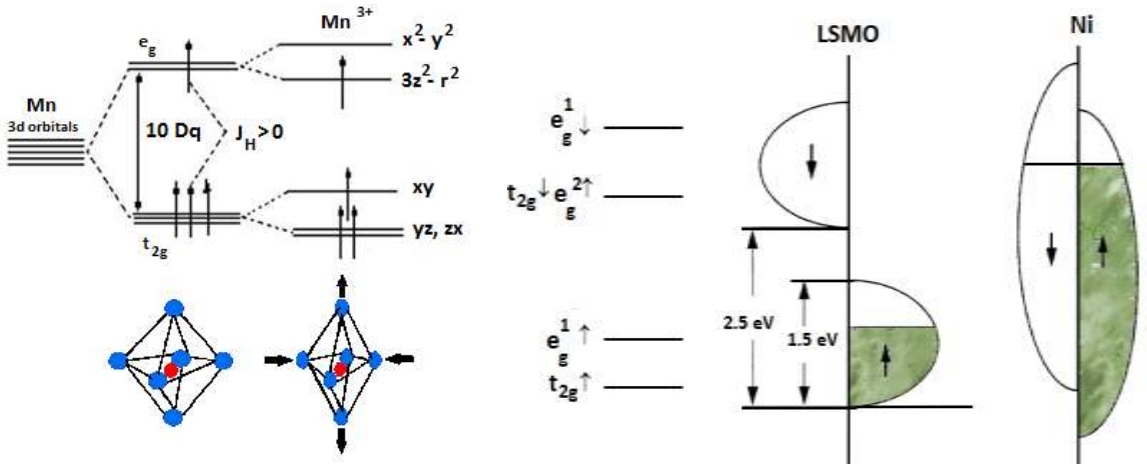

Figure 2. (a) Crystal field splitting of the Mn ion *d*-levels and electronic occupation of the mixed-valence Mn ions. The degeneracy of the e_g and t_{2g} levels is lifted by an in-plane contraction and out-of-plane elongation of the oxygen octahedron. (b) Schematic illustration of the density of states of LSMO and Ni showing the fully spin-polarized conduction band of LSMO. Adapted from Ref. 8 [Dagotto A et al., 2001 *Phys. Rep.* **344** 1] and 33 [Haghiri-Gosnet A -M and Renard J -P 2003 *J. Phys. D: Appl. Phys.* **36** R127].

The phase diagram of mixed-valence LSMO [8, 15] is shown in Fig. 3. For low hole doping ($x < 0.1$), LSMO is an antiferromagnetic insulator (AFM-I). With increasing hole doping, first a ferromagnetic insulating (FM-I) ($x < 0.2$) and eventually a ferromagnetic metallic (FM-M) ($x = 0.2 – 0.4$) ground state is stabilized. For $x = 0.3$, a metal-insulator transition is observed at T_{MI}, which is close to T_C. Both the metal-insulator and the paramagnetic-ferromagnetic phase transitions are connected to the electronic distribution of spin-up and spin-down states and the width of the impurity band. The magnetic and transport properties in this correlated electron system are essentially influenced by the size of the *A*-site cations which controls the tolerance factor, the average Mn-O bond length, and the Mn-O-Mn bond angle of the MnO_6 octahedra. The two transition temperatures T_{MI} and T_C can either coincide (for single crystals or epitaxial thin films) or vary substantially depending on the presence of structural defects and grain boundaries.

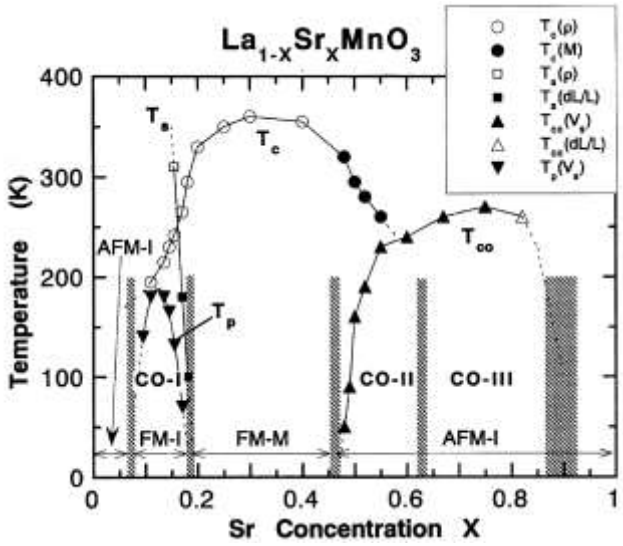

Figure 3. Phase diagram of $La_{1-x}Sr_xMnO_3$, reproduced with permission from Ref. 15 [Fujishiro H, Fukase T and Ikebe M, 1998 *J. Phys. Soc. Jpn.* **67** 2582].

The regime in which ferromagnetism and metallic conduction coexist is generally explained by double exchange (*DE*) [16, 17] between localized 3*d* magnetic moments with strong on-site Hund's coupling. Hopping of e_g electrons between adjacent Mn^{3+} and Mn^{4+} along the Mn-O-Mn chains governs both ferromagnetism and metallic transport. The hopping probability is largest when the Mn spins are aligned parallel. Anderson and Hasegawa have shown that the transfer integral varies as the cosine of the angle between neighboring spins [18]. Hence, charge carriers can move easily in the ferromagnetic phase while they get localized due to randomly aligned Mn spins when the manganite is paramagnetic. Mechanisms that are capable of modifying the spin alignment, such as magnetic field or temperature, can therefore alter the carrier mobility and the resulting electrical conductivity. With decreasing temperature, the combined itinerant and local-moment system lowers its total energy by ferromagnetic spin alignment and by allowing the itinerant electrons to gain kinetic energy [19]. However, Millis et al. [20-22] have shown that a Hamiltonian incorporating the *DE* interaction alone cannot explain CMR in manganites [8]. It was proposed that in addition to *DE*, an electron–phonon coupling term dictates electronic transport, which is expected for a system where electrons hop between Mn^{3+} and Mn^{4+} ions. Hole doping of the system replaces $Mn^{3+}(d^4)$ by $Mn^{4+}(d^3)$ which, in the dilute limit, is associated with large *JT* coupling. The *DE* model with the inclusion of *JT* distortions explains the CMR effect and the high temperature paramagnetic phase in LSMO and other manganites in general.

In LSMO, different MR mechanisms are active including CMR and low-field magnetoresistance (LFMR). CMR is associated with the suppression of spin fluctuations in an applied magnetic field and therefore a fairly large magnetic field (a few Tesla) is required [8]. LFMR is due to the suppression of spin-

dependent scattering at grain boundaries or tunneling between grains, which requires a small magnetic field that is comparable to the coercivity [23]. In the low temperature ferromagnetic phase (below T_C), the conduction electrons are almost completely polarized inside a magnetic domain resulting in easy transfer of electrons within the Mn–O–Mn chains. Hence, in single crystals or epitaxial thin films the manganite resistance does not change substantially in a small applied magnetic field. However, for polycrystalline bulk materials or thin films, the differently aligned magnetic domains and the grain boundaries can act as insulating scattering centers for spin-polarized electrons, which enhances the zero-field resistivity. There are two different effects related to LFMR. i) Electrons from one magnetic domain hop to another magnetic domain through an intermediate insulating layer by a spin-dependent tunneling process (<500mT) and ii) suppression of spin fluctuations at grain boundaries at larger field (>500 mT). The probability of spin-dependent tunneling depends strongly on the spin states of neighboring grains. At the coercive field, half of the domains switch their magnetic orientation. Hence, the tunneling probability of electrons is smallest at H_c and the electrical resistance peaks. After successive magnetization reversal into the direction of the external magnetic field, the tunneling probability again increases leading to a decrease of the electrical resistance. There are reports of up to 20% LFMR in polycrystalline LSMO thin films on single crystal (100) yttria-stabilized zirconia substrates [24]. The suppression of spin fluctuations at grain boundaries by a moderate magnetic field also contributes to the negative MR effect.

The temperature dependence of electrical conductivity in bulk and thin films of LSMO has been described by different models. In the low temperature ferromagnetic phase, the resistivity of LSMO has been fitted with equations of the form [25]:

$$\rho = \rho_0 + \rho_2 T^2 \quad (1)$$

$$\rho = \rho_0 + \rho_{2.5} T^{2.5} \quad (2)$$

$$\rho = \rho_0 + \rho_2 T^2 + \rho_{4.5} T^{4.5} \quad (3)$$

where ρ_0 is the resistivity due to temperature-independent scattering on impurities, defects, domains-walls and grain boundaries. Generally, ρ_0 decreases significantly in an applied magnetic field due to an improved spin alignment at grain boundaries and domain walls. The temperature dependence of the resistivity originates from different scattering sources. For example, Urushibara et al. [25] showed that the resistivity of single crystal LSMO can be fitted well below 200 K using Eq. 1. In this case, the T^2 term predominantly accounts for electron-electron scattering. Additional electron-magnon scattering can be taken into account by the introduction of a $\rho \alpha T^{4.5}$ term (Eq. 3), which is typical for double-exchange systems [Ref. 19 and references therein]. However, Eq. 2 provides a better fit to some experimental data. Finally, electron-phonon scattering does increase the resistivity of LSMO at high temperatures. Just like ρ_0, the temperature-

dependent terms (ρ_2, $\rho_{2.5}$ or $\rho_{4.5}$) decrease in a magnetic field. Snyder et al. [26] suggested that the decrease of ρ_2 is proportional to $H^{-1/3}$, which implies that a reduction of spin fluctuations suppresses electron-electron scattering in LSMO.

4. Control of $La_{1-x}Sr_xMnO_3$ properties by pulsed laser deposition

Pulsed laser deposition is a thin-film ablation technique based on laser-matter interactions. In a PLD setup, a short and high-energy laser pulse is focused on a target. The intense local heating induces ejection of target ions into a plasma plume. The substrate, placed at an optimum distance from the target, receives the plasma ions and under the right deposition conditions (temperature, background gas pressure, laser fluence, and pulse repetition rate) high quality films can be grown. The stoichiometry of complex multi-element materials is conserved during the PLD process. In addition, PLD is a powerful technique for obtaining smooth defect free interfaces between thin films, which is of particular interest for spintronic structures.

The magnetic and electrical transport properties of LSMO are controlled by lattice-charge-spin coupling, which is very sensitive to phase and structural order, oxygen stoichiometry, and lattice distortions induced by doping [27-29]. In thin films, the physical properties are further influenced by low and high angle grain boundaries (polycrystalline growth) and lattice strain. For PLD of LSMO thin films, mainly excimer lasers (Nd:YAG laser, KrF (248 nm) and ArF (193nm)) are used. The laser fluence and pulse repetition rate for optimal LSMO films depend on the composition, substrate, and deposition temperature. High deposition temperatures (> 650°C) and post-deposition annealing under a controlled oxygen pressure are generally required for the growth of high-quality LSMO films. Although the optimum deposition parameters vary for films grown by different groups, typical growth parameters for LSMO thin films are a deposition temperature of 700 - 800°C, an oxygen pressure of about 0.25 Torr, a laser repetition rate of 5 - 10 Hz and a laser fluence of 2 – 2.5 J /cm^2.

For spintronic applications, the large spin polarization of LSMO is a desirable property. In addition, a high T_C, good metallic conductivity, and atomically smooth interfaces are often essential for practical devices. Because strain control in thin LSMO films is vital for obtaining optimal properties, the effects of strain have been studied extensively [30-32]. More details can for example be found in Ref. 33 and references therein. Various single-crystal substrates including $SrTiO_3$ (STO), $LaAlO_3$ (LAO), $NdGaO_3$ (NGO), and MgO have been used for PLD of LSMO. Because of the small lattice mismatch between LSMO and these substrates (except for MgO), the lattice strain is not released easily. For example, 20 – 30 nm thick LSMO films on STO are still considerably strained and bulk-like lattice parameters are only obtained for considerably thicker films. The MnO_6 octahedra of strained LSMO are distorted and the hopping probabilities of e_g electrons are restricted. Localization of e_g electrons reduces the ferromagnetic

interactions and it enhances the electrical resistivity of thin LSMO films, two effects that are not desirable for spintronic structures.

Other factors that control the magnetic and electrical transport properties of LSMO are film composition, oxygen stoichiometry and crystal orientation [34-38]. The composition and oxygen content mainly affect the saturation moment and the transition temperature, whereas lattice strain and film texture can also induce magnetic anisotropy [39, 40]. Moreover, LSMO films with a polycrystalline texture can exhibit large LFMR and a large dielectric constant due to the presence of high and low angle grain boundaries.

To illustrate the influence of substrate selection and PLD parameters on the structural, magnetic and electrical properties of LSMO films, we discuss some of our results below [41, 42]. In the experiments, the LSMO films were systematically grown on three different single-crystal substrates (STO (001), NGO (001), MgO (001)) under a variety of PLD conditions. X-ray diffraction pole figures ($\varphi - \psi$ scans) of the (110) reflection at $2\theta = 32.76°$ are shown in Fig. 4. Obviously, different crystal orientations are obtained in most of the samples. Only the films grown at 700°C (indicated by number 5) and a LSMO thickness of about 200 nm on MgO and STO are fully epitaxial. All other films contain additional crystal orientations with pseudocubic axes at 10°, 13°, 16° and 27° angles with respect to the substrate [001] direction. In addition, the reflections from LSMO films on MgO are much wider than those from STO and NGO samples, indicating the presence of low angle grain boundaries with single grain orientation.

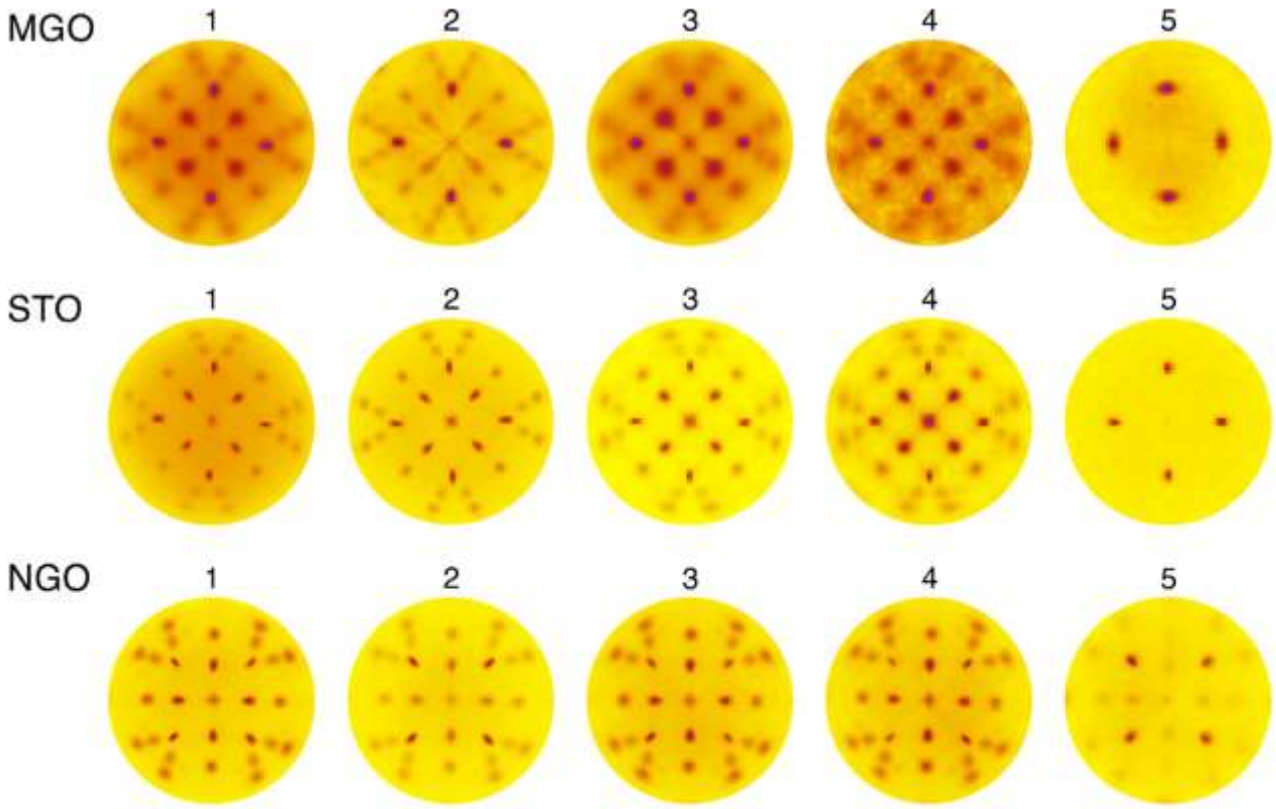

Figure 4. X-ray diffraction pole figures of the LSMO (110) reflection at 2θ = 32.76° on MgO, STO and NGO substrates with a (001) orientation. The PLD parameters for samples indicated by No. 1 are; growth temperature T_S = 780 °C, laser pulse frequency f = 5 Hz, and LSMO film thickness t = 400 nm. For 2, T_S = 780 °C, f = 5 Hz, and t = 200 nm. For 3, T_S = 780 °C, f = 10 Hz, and t = 400 nm. For 4, T_S = 780 °C, f = 10 Hz, and t = 500 nm. For 5, T_S = 700 °C, f = 10 Hz, and t = 200 nm. Reprinted from *J. Alloys and Compounds,* **512,** Majumdar S et al., Stress and defect induced enhanced low field magnetoresistance and dielectric constant in $La_{0.7}Sr_{0.3}MnO_3$ thin films, 332, © (2012), with permission from Elsevier.

Magnetic measurements on LSMO/MgO (001) clearly indicate that the ferromagnetic-paramagnetic phase transition of LSMO is considerably broader than that of comparable films on STO and NGO (Fig. 5). The broadening of the magnetic transition is accompanied by a metal-insulator transition at a temperature well below T_C. Both effects are explained by the formation of (001) and (211)-oriented grains during PLD of LSMO on MgO [42]. For LSMO films on STO and NGO substrates, the magnetic properties do depend less on PLD conditions and film thickness, although the T_C of 200 nm films on STO (342 K) is approximately 10 K less than for 400 nm films. The reduction of T_C is ascribed to compressive film strain. The largest LFMR effect (17%) is obtained for the thickest LSMO film on MgO while the LFMR is only 1% for epitaxial films on STO and nearly epitaxial films on NGO. These results indicate that tunneling through grain boundaries contributes significantly to the conduction of polycrystalline LSMO films on MgO. Finally, LSMO films on MgO (001) with a high density of grain boundaries possess a large dielectric constant (ε_r') [41, 42]. At room temperature, ε_r' remains large up to a frequency of a few kHz. This behavior is explained by a variation of the conductivity and capacitance of grains and grain boundaries, which leads to Maxwell–Wagner-type polarization and the formation of a Schottky barrier at the interface. The ε_r' of epitaxial LSMO films on STO (001) on the other hand, remains relatively constant up to MHz frequencies. In this system, lattice strain mainly influences the evolution of ε_r'.

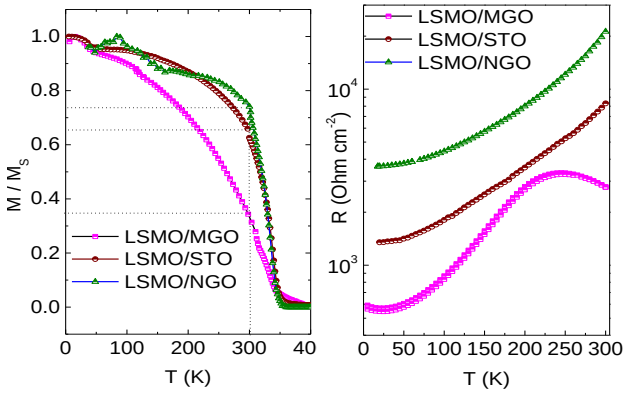

Figure 5. Temperature dependence of field cooled magnetization (left) and sheet-resistance of LSMO films (right) on MgO, STO and NGO substrates grown under the same experimental conditions as sample 3 in Fig. 4. Adapted from Ref. 43 [Majumdar S et al., 2008 *J. Appl. Phys.* **104** 033910].

The coexistence of ferromagnetism with defect-induced LFMR and a large dielectric constant opens up new routes for a variety of interesting applications. For spintronics, however, epitaxial and defect free LSMO films on lattice-matched substrates are more desirable. One drawback of LSMO-based spintronic structures is the relatively low T_C. Although the T_C of LSMO thin films is about 360 K, it has been reported that it already starts to lose its spin polarization at ≈200 K [44], especially near the surface of the LSMO film. Consequently, only a current with small spin polarization can be generated in LSMO-based spintronic devices at room temperature, which poses a serious challenge for practical applications. Also, the tunneling magnetoresistance (TMR) of magnetic tunnel junctions (MTJs) with LSMO electrodes is often smaller than expected, which suggests that the LSMO interface layer is not fully spin-polarized at the Fermi level. The reduction of spin polarization might be due to LSMO-tunnel barrier interactions. In fact, some studies indicate that LSMO can lose its half-metallicity in contact with a STO (001) substrate [45, 46]. According to polar discontinuity theory [47, 48], STO is composed of alternating SrO and TiO_2 planes while (001) oriented LSMO is deposited as alternating layers of $(La_{0.67}Sr_{0.33}O)^{0.67+}$ and $(MnO_2)^{0.67-}$. Thus, the LSMO layers are charged while STO is charge-neutral. The polar discontinuity that occurs at the STO-LSMO interface leads to an electronic redistribution, which either reduces or enhances the charge carrier density in the interfacial layers of LSMO. As a result, the population of the e_g orbitals changes and via the *DE* mechanism this can alter the electrical conductivity and magnetic properties of the LSMO interface. To avoid detrimental effects due to polar discontinuities, interface engineering of LSMO-STO heterostructures has been suggested as a possible solution [49, 50].

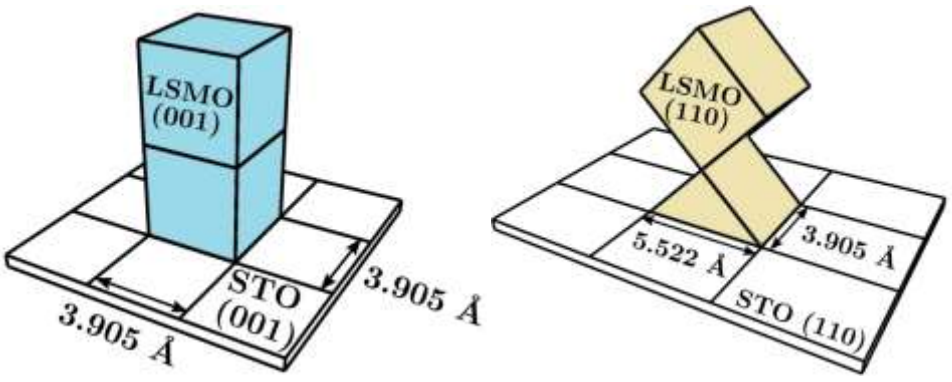

Figure 6. Schematic illustration of the LSMO lattice orientation on STO (001) and STO (110) substrates. Adapted from Ref. 51 [Majumdar S et al. 2013 *J. Phys.: Condens Mat.* **25** 376003].

One route towards interface engineering is based on the growth of LSMO films on substrates with different crystal orientation. For example, LSMO on (110)-oriented STO substrates exhibits a completely different interface structure than LSMO on STO (001) (Fig. 6). In the (110) system, the STO is composed of alternating $SrTiO^{4+}$ and O_2^{4-} planes. Since LSMO (110) contains alternating layers of $La_{0.67}Sr_{0.33}MnO^{4+}$ and O_2^{4-}, a polar discontinuity is avoided and the magnetization and spin polarization of the interfacial layers can be preserved. Experiments indeed show that (110)-oriented LSMO films possess a larger magnetic moment and higher T_C (increase of about 15 K) compared to (001) oriented films [51]. Moreover, recent x-ray photoelectron spectroscopy (XPS) and high kinetic energy XPS studies indicate that LSMO films on STO (001) are under larger tensile strain, due to strain effects in both the [100] and [010] in-plane directions. This not only affects the LSMO lattice parameters but also the angle between the unit cell axes. For (110)-oriented LSMO, strain effects along the [001] and [1 $\bar{1}$0] directions affect the LSMO unit cell less. As a result, LSMO (110) films are more relaxed. This in turn leads to a smaller distortion of the MnO_6 octahedra and a higher population of Mn^{4+} ions, which via improved *DE* interactions enhances the magnetic properties of LSMO.

5. Applications of $La_{1-x}Sr_xMnO_3$ in spintronics

a. Magnetic tunnel junctions (MTJ)

The ever-increasing demand for high-density magnetic data storage on computer hard-disk drives has motivated extensive research on magnetic tunnel junctions (MTJs) that exhibit large tunneling magnetoresistance (TMR) at room temperature. Moreover, MTJs form the storage cells in non-volatile magnetic random access memories (MRAMs). MTJs consist of a multilayer structure with two ferromagnetic electrodes that are separated by a thin insulating tunnel barrier. In most cases, dielectric oxides such as Al_2O_3 and MgO provide the necessary potential for quantum-mechanical tunneling of electrons between the two ferromagnetic layers. The TMR effect is a measure of the relative change in tunnel barrier resistance upon magnetization reversal in one of the electrodes. The effect is largest when the alignment of the magnetic moments on either side of the tunnel barrier switches from parallel to antiparallel or vice versa. TMR originates from an imbalance between the number of majority and minority electrons that contribute to the tunneling current. The spin-polarized band structure of the electrodes and spin filtering within the tunnel barrier can both contribute to the magnitude of TMR. When the influence of the tunnel barrier is negligible (e.g. for MTJs with amorphous Al_2O_3), the TMR effect is approximated by Julliere's formula [52]:

$$\mathrm{TMR} = \frac{R_{AP} - R_P}{R_P} * 100\% = \frac{2P_1P_2}{1-P_1P_2} \qquad (4)$$

where R_{AP} and R_P are the tunnel barrier resistance for antiparallel and parallel aligned magnetic moments and P_1 and P_2 indicate the spin polarization of the electrodes. The latter quantity is often specified as:

$$P = \frac{N_{\uparrow}(E_F) - N_{\downarrow}(E_F)}{N_{\uparrow}(E_F) + N_{\downarrow}(E_F)} \qquad (5)$$

with $N_{\uparrow}$ and $N_{\downarrow}$ indicating the density of majority and minority electrons at the Fermi level.

Because of its half-metallic character, LSMO has been explored as electrode material for MTJs (see for example Refs. 53 and 54 for details). In most cases, the LSMO and barrier layers are grown by PLD. The first demonstration of TMR using LSMO electrodes was reported by a research group at IBM [55, 56]. The best results in this study were obtained using optimally doped $La_{2/3}Sr_{1/3}MnO_3$ electrodes and 3 - 6 nm thick STO tunnel barriers. The junctions, which were fabricated using a combination of optical lithography and ion-beam etching, showed a TMR of 83% at 4.2 K [55]. According to Julliere's formula (Eq. [4]), this corresponds to a LSMO spin polarization of 54%. In subsequent years, considerably larger TMR values for LSMO-based MTJs were reported in literature [57, 58]. For example, Bowen and coworkers reported a low-temperature TMR of 1850% for MTJs with a LSMO/STO/LSMO structure (Fig. 7) [57]. A spin polarization of 95% can be extracted from these experiments, which confirms the half-metallicity of LSMO.

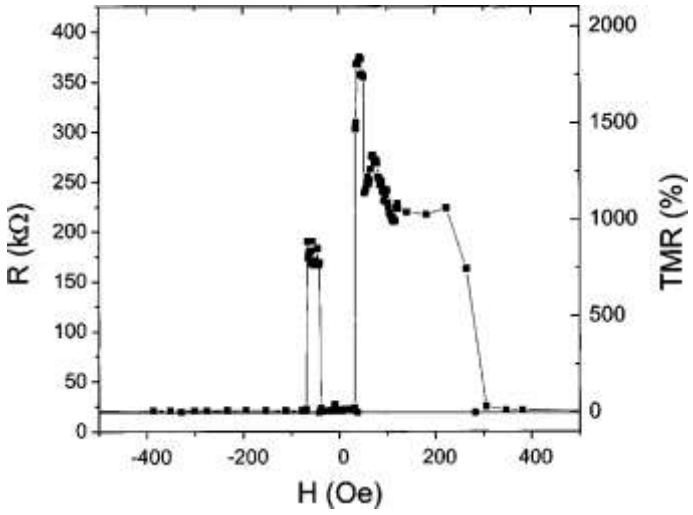

Figure 7. TMR versus magnetic field curve for a MTJ with a LSMO/STO/LSMO structure at 4 K. Reprinted with permission from Bowen M et al. 2003 *Appl. Phys. Lett.* **82** 233 © [2003], American Institute of Physics.

Despite these promising results, LSMO electrodes exhibit some detrimental properties. In particular, the TMR effect of LSMO-based MTJs tends to decrease sharply with temperature, becoming negligible at room temperature [44]. Moreover, the MTJ resistance does not scale linearly with the inverse of the junction area [23], which suggest that electron tunneling between LSMO electrodes is inhomogeneous. Finally, MTJs with LSMO electrodes often exhibit an irregular switching behavior (Fig. 7). In the remainder of this section, the temperature and bias voltage dependence of LSMO-based MTJs are briefly discussed. We also elaborate on the observation of inverse TMR effects and interface engineering strategies to overcome some of the drawbacks of LSMO.

Temperature dependence: Although LSMO-based MTJs often show very large TMR ratios at low temperature, the effect decreases considerably at elevated temperatures irrespective of tunnel barrier material [59-62]. Especially above $T \approx 200$ K, sharp decays of TMR are often observed [44]. Since this characteristic feature occurs well below the T_C of LSMO films (≈360 K), it raises questions regarding the breakdown of half-metallicity. Polar discontinuity theory [47, 48] suggests the formation of a magnetically dead layer at the LSMO-STO interface, which is detrimental for the ferromagnetic properties and hence spin polarization of LSMO. In their study on LSMO-based MTJs with LAO and STO tunnel barriers, Garcia et al. concluded that the spin polarization at the surface of LSMO decays much faster than in the bulk due to the discontinuation of oxygen bonds [44]. In this picture, the distortion of the MnO_6 octahedra by dangling bonds acts as a localization center for e_g electrons and this results in a deterioration of the magnetic and electronic properties (Fig. 8). In experiments, the modified magnetic and electronic properties are often manifested by a decrease of T_C and T_{MI}, a decrease of the saturation magnetization, and an increase of the resistivity and low temperature magnetoresistance. At LSMO-oxide barrier interfaces the oxygen bonds are better preserved and, hence, the interface spin polarization is considerably larger compared to that of free LSMO surfaces. However, both transport and spectroscopic studies indicate that even with better preserved oxygen bonds the spin polarization of the LSMO/oxide barrier interface vanishes completely at about 300 K. Large TMR values at room temperature remain therefore elusive for MTJs with LSMO electrodes.

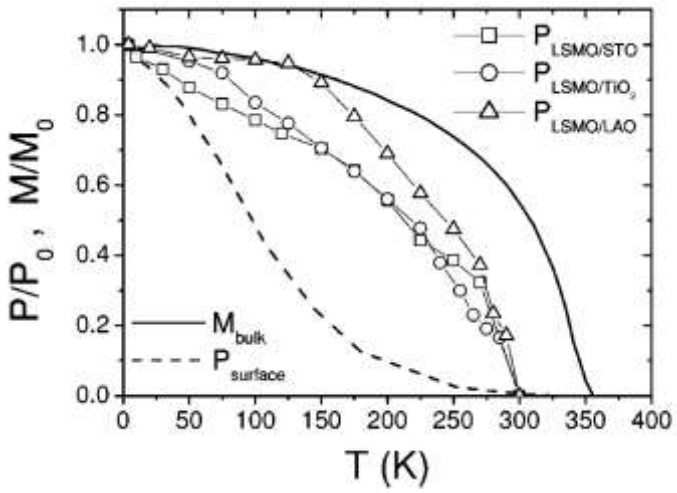

Figure 8. Temperature dependence of the bulk magnetization and surface spin polarization of free LSMO and the interface spin polarization of LSMO in contact with three different oxide tunnel barriers. Reprinted with permission from Garcia V et al. 2004 *Phys. Rev. B* **69** 052403 © [2004], American Physical Society.

Bias voltage dependence: Another striking feature of LSMO-based MTJs is a fast decay of the TMR effect with increasing bias voltage, especially in the low (≤ 0.2 V) bias range (Fig. 9) [63-65]. This strong bias dependence is accompanied by a zero-bias anomaly in the conductance curves. Gu et al. theoretically

studied the anomaly and they proposed that the tunnel barrier conductance is proportional to $|V|^{3/2}$ due to *DE* interactions in LSMO [66]. They showed that the stimulation of spin excitations, caused by strong Hund's coupling between the conduction e_g electrons and the localized quantum spins of the LSMO ions, assists electron tunneling even for antiparallel aligned electrodes. As a result, an extra tunneling conductance and a decrease of TMR are obtained. These findings are also confirmed by experimental studies [55, 65]. At a bias voltage of about 350 mV, a plateau in the TMR curve is generally observed, which is followed by another sharp decrease beyond 400 mV (Fig. 9) [65]. The point of inflection can be interpreted as the onset of electron tunneling into the minority conduction band of LSMO. Based on this hypothesis, one can determine the position of the minority LSMO band from TMR measurements. The obtained value of 380 mV corresponds well with spin-polarized inverse photoemission results [67]. Exchange biasing of LSMO electrodes have been also shown using antiferromagnetic $La_{0.45}Sr_{0.55}MnO_3$ in an MTJ with structure $La_{0.45}Sr_{0.55}MnO_3$/LSMO/STO/Co and robust exchange bias with exchange energy of 0.13 erg cm^{-2} at the interface between antiferromagnetic $La_{0.45}Sr_{0.55}MnO_3$ and ferromagnetic LSMO is reported [68]. More details on the bias dependence of LSMO-based MTJs are discussed elsewhere [69].

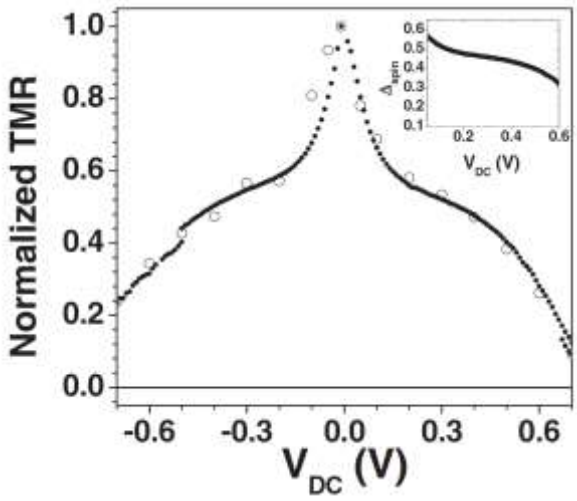

Figure 9. Bias dependence of a LSMO/STO(2.8 nm)/LSMO MTJ (normalized to its value at 10 mV) at 4.2 K. The inset shows the spin asymmetry, defined as $\Delta_{spin} = (I_P - I_{AP})/ (I_P + I_{AP})$, in this bias range. Reprinted with permission from Bowen M et al. 2005 *Phys. Rev. Lett.* **95** 137203 © [2004], American Physical Society.

Inverse TMR: Depending on the choice of barrier material and the applied bias voltage, both normal and inverse TMR effects can be observed in LSMO-based MTJs. De Teressa et al. [70] showed that for a LSMO and Co electrode, normal TMR is observed for an Al_2O_3 (ALO) tunnel barrier while for STO and $Ce_{0.69}La_{0.31}O_3$ (CLO) barriers the TMR response is inversed (Fig. 10). In the latter case, insertion of a thin ALO layer between the STO tunnel barrier and the Co electrode changes the sign of the TMR effect, but insertion of ALO between the STO barrier and LSMO does not alter the TMR response. These results are explained by a

change in tunneling spin polarization due to different bonding at the dielectric oxide-Co interfaces. The effective polarization of Co is negative for STO or CLO barriers, but positive for ALO. The negative tunneling spin polarization of Co indicates preferential transmission of *d* electrons from the Co-STO and Co-CLO interfaces, while the positive polarization is due to predominant tunneling of *s* electrons from the Co-ALO interface. Consequently, inverse and normal TMR effects are observed for tunneling of *d* electrons and *s* electrons, respectively. Inverse TMR effects have also been observed in LSMO-based MTJs with a $Co_{90}Fe_{10}$ [71, 72], CoFeB [73], and Fe or $Ni_{40}Fe_{60}$ [74] counter electrode.

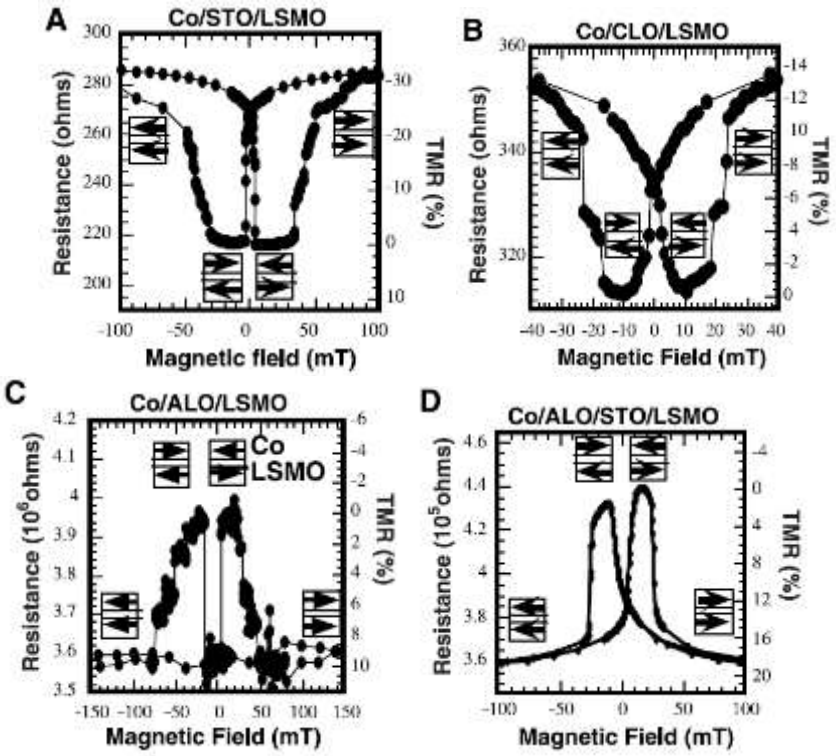

Figure 10. TMR response of MTJs with a LSMO and Co electrode and a STO (a), CLO (b), ALO (c) or hybrid ALO/STO (d) tunnel barrier at 40 K. Reprinted with permission from De Teresa J M et al., 1999 *Science* **286** 507. Reprinted with permission from AAAS.

Interface engineering: Several interface engineering techniques have been explored to improve the performance of LSMO-based MTJs. Due to a polar discontinuity, a STO tunnel barrier donates holes to LSMO electrodes [75]. The insertion of 2 unit cells of $LaMnO_3$ between LSMO and STO can compensate for charge transfer at LSMO/STO interfaces [76]. Experiments indicate that the magnetic properties of this engineered interface are better, however, significant improvements of the TMR response and the temperature stability have not been demonstrated yet [77]. Other routes that have been explored include the use of LAO tunnel barriers [76] or the growth of more stable LSMO (110) electrodes [78]. Also in these cases, only limited enhancements of MTJ properties are obtained.

b. Multiferroic tunnel junctions (MFTJ)

One of the recent trends in spintronics is the exploration of electric-field controlled magnetism. Materials that combine magnetic and ferroelectric phases, or so-called multiferroics, offer this desirable property via magneto-electric (ME) coupling between two ferroically ordered states. Unfortunately, single-phase multiferroic materials are rare and their application potential is often limited by low ordering temperatures, small ferroelectric polarization or magnetization, or weak ME coupling. As an alternative, studies on multiferroic heterostructures have greatly intensified in recent years (see e.g. Refs. 79 and 80 for reviews). In a multiferroic heterostructures, magnetic and ferroelectric films are artificially assembled and the ME coupling originates from direct or indirect interactions at the interfaces. Each material constituent of a multiferroic heterostructure can be independently optimized for high temperature operation, which facilitates their integration into practical devices. Moreover, since a wide variety of magnetic and ferroelectric materials are available, the nature and strength of ME interactions can be systematically altered and maximized. This has led to the engineering of large ME responses that exceed those of single-phase multiferroic materials by several orders of magnitude. Complex oxide materials are of particular interest for multiferroic heterostructures because their physical properties are very sensitive to external parameters including strain and electric fields. Indeed, electric-field control of LSMO properties has been achieved by PLD growth onto piezoelectric substrates [81 - 85]. In these structures, an electrically activated piezostrain is transferred to the LSMO layer, which alters the magnetic and electrical transport properties. Direct electric-field effects have been obtained in systems where LSMO is directly coupled to a ferroelectric material. Here, out-of-plane polarization reversal in the ferroelectric causes charge accumulation or depletion in the interfacial layers of LSMO, which for an appropriately selected doping concentration *x* can lead to magnetic and electric phase transitions. Finally, LSMO has been used extensively as bottom electrode in multiferroic tunnel junctions (MFTJs). In this section, we will briefly review the physics of MFTJs and electric-field controlled LSMO phase transitions.

MFTJs consist of two ferromagnetic electrodes separated by an insulating ferroelectric tunnel barrier. In most cases, the ferroelectric material is $BaTiO_3$ (BTO), $PbTiO_3$ (PTO) or $PbZr_{0.2}Ti_{0.8}O_3$ (PZT). Tunnel junctions with a single-phase multiferroic tunnel barrier have also been studied [86]. In all junctions, PLD is used to grow the LSMO bottom electrode. Besides the necessary electrical conductivity, LSMO provides a compressive lattice strain to the BTO, PTO or PZT tunnel barrier which stabilizes the out-of-plane ferroelectric polarization. Using piezo-response force microscopy (PFM), Garcia et al. have shown that the ferroelectric polarization of ultrathin BTO films on LSMO can be retained down to a film thickness of only 1 nm (Fig. 11) [87]. Reversal of the polarization in MFTJs changes the tunnel barrier resistance [87 - 90]. This effect, which has been labeled as tunneling electroresistance (TER), can have different origins [91]. In junctions with a metallic top electrode (e.g. Co, Fe etc.), TER is often explained by an incomplete screening

of the polarization charges at the barrier/electrode interfaces, which for inherently different electrode materials leads to an asymmetric deformation of the barrier potential profile [92, 93]. In this case, reversal of the barrier polarization produces distinctive average barrier heights and consequently two different tunnel barrier resistances. This scenario is supported by an exponential increase of the TER effect with tunnel barrier thickness [87]. The TER effect of MFTJs can be considerably larger than the TMR of conventional MTJs. The maximum TMR effect at room temperature is about 600% for MgO-based MTJs with CoFeB electrodes [94], which correspond to an OFF/ON ratio of 7. However, for MFTJs with a $La_{0.67}Sr_{0.33}MnO_3$ bottom electrode, a BTO tunnel barrier, and a Co top electrode, OFF/ON ratios as high as 100 have been obtained at room temperature (Fig. 12) [88]. Moreover, ferroelectric switching between two resistance states only requires a current density of about 1 x 10^4 A cm^{-2}, which is considerably smaller than the critical current density for spin-transfer torque writing in MTJs (> 1 x 10^6 A cm^{-2}). The large, stable, and reproducible TER effect underpins the potential of FTJs for data storage applications.

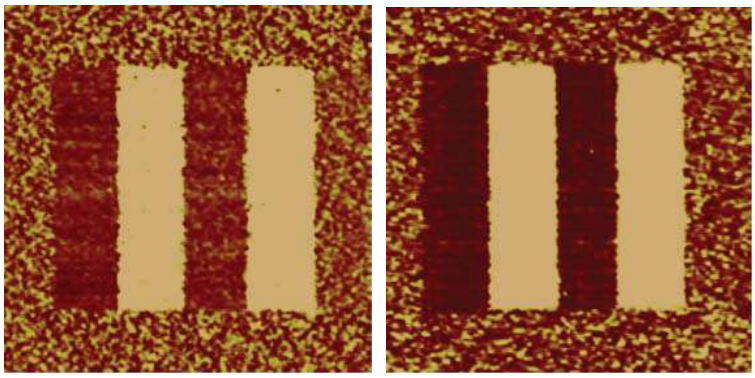

Figure 11. Evidence of ferroelectricity in 1 nm (left) and 3 nm (right) thick BTO films on LSMO. Reprinted by permission from Macmillan Publishers Ltd: [*Nature*] Garcia V et al., 2009 *Nature* **81** 460, copyright (2009).

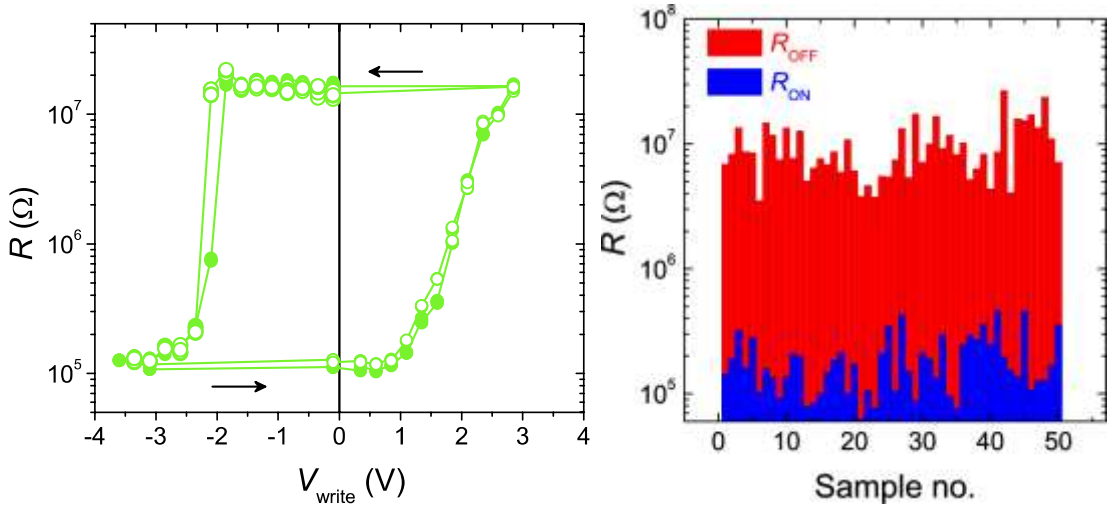

Figure 12. (Left) Junction resistance as a function of bias voltage for an MFTJ with a LSMO/BTO/Co structure. (Right) Reproducible switching between the ON and OFF resistance states of 50 different

junctions. Reprinted by permission from Macmillan Publishers Ltd: [*Nature Nanotech.*] Chanthbouala A et al., 2012 *Nature Nanotech.* **7** 101, copyright (2012).

The TER effect is not limited to MFTJs because it does not rely on the electrodes being magnetic. Large electrical responses have also been obtained for non-magnetic top contacts [95 - 97]. More generally, such structures are often referred to as ferroelectric tunnel junction (FTJ). In addition to the TER effect, however, MFTJs also exhibit a TMR response. The magnitude and even sign of the TMR effect can change upon polarization reversal in the tunnel barrier [98 - 100]. As an example, Fig. 13 shows experimental data of a Co/PZT(3.2 nm)/LSMO junction [98]. In this experiment, switching of the polarization from pointing towards the Co to pointing towards the LSMO electrode by a +3 V bias voltage pulse changes the TMR response from -7% to +5% at 10 K. An opposite effect is measured when a bias pulse of -3 V is applied. This modification of the TMR effect is attributed to either an anti-aligned induced magnetic moment on the Ti ions at the Co interface or a spin-dependent screening effect in the LSMO interfacial layers. Support for the first scenario has been obtained by x-ray resonant magnetic scattering measurements [99] and first-principles calculations based on density-functional theory [101].

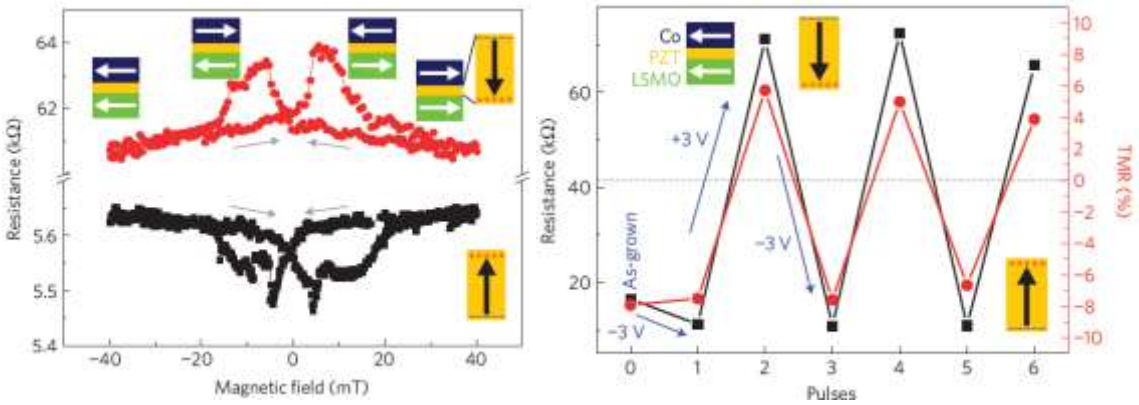

Figure 13. (Left) TMR response of a Co/PZT(3.2 nm)/LSMO junction at 50 K in the as-grown state (black squares) and after polarization switching with a +3V voltage pulse (red circles). The polarization state of the barrier as well as the magnetization of the two electrodes are schematically shown for each non-volatile state. (Right) Resistance (black squares) and TMR (red circles) after successive switching with 3 V pulses for a different junction at 10 K. Reprinted by permission from Macmillan Publishers Ltd: [*Nature Mater.*] Pantel D et al., 2012 *Nature Mater.* **11** 289, copyright (2012).

Besides LSMO/ferroelectric barrier/metallic electrode junctions, large TER effects have also been obtained in all-oxide MFTJs. Recently, Yin et al. reported on a TER response of 5000% at 40 K in PLD grown 50 nm LSMO/3 nm BTO/0.4 – 2 nm $La_{0.5}Ca_{0.5}MnO_3$ (LCMO)/30 nm LSMO junction [89]. The origin of this

effect is attributed to an electric-field induced metal-insulator transition in the LCMO layer, which is driven by charge modulation. As the junction resistance depends exponentially on the barrier width, large effects are readily obtained when only a few atomic layers of the LCMO are affected by polarization reversal. The ability to induce a phase transition in the interfacial layers of thin-film manganites with appropriate doping concentration is supported by DFT calculations and experiments. Theoretical work by Tsymbal and co-workers indicates that the magnetic structure of the interfacial layers of $La_{0.5}Sr_{0.5}MnO_3$ changes from ferromagnetic to antiferromagnetic when the polarization in a neighboring BTO film is rotated away from the LSMO/BTO interface [102]. A similar effect is calculated for $La_{0.5}Ca_{0.5}MnO_3$ [89]. According to the phase diagram of LSMO and LCMO, the ferromagnetic-to-antiferromagnetic transition is closely associated with a metal-insulator transition (Fig. 3).

Additional experimental evidence for strong electric-field effects in LSMO can also be found in literature. For example, Hong et al. demonstrated that the temperature of magnetic phase transitions and the MR response change upon polarization reversal in LSMO/PZT field-effect structures [103]. Magneto-optical Kerr effect measurements on 250 nm PZT/4 nm LSMO bilayers confirm this observation [104]. In the latter study, it is also shown that the magnetization of LSMO changes when the polarization of an adjacent PZT film is reversed between two out-of-plane states. The origin of this effect was studied in detail by Vaz et al. using x-ray absorption near edge spectroscopy (XANES) [105]. In their experiments, large shifts in the absorption edge of Mn were observed, indicating a change of Mn valency due to charge carrier modulation in LSMO. Holes are depleted from the LSMO interface region when the polarization of the PZT layer points towards the LSMO film, whereas hole accumulation occurs when the polarization points in the opposite direction. These electrostatic modifications are analogous to chemical doping of LSMO. Polarization reversal can therefore induce large magnetic and electrical transport effects when the LSMO doping concentration is positioned near one of the phase transitions. For example, recent experiments by Lu et al. indicate that electric-field control over the ferromagnetic-paramagnetic phase transition is obtained for PLD-grown $La_{0.67}Sr_{0.33}MnO_3$ films at room temperature [106].

The recent progress on electric-field controlled effects in LSMO and LSMO-based MFTJs holds a great promise for practical device applications, especially since significant and reproducible effects can be obtained at room temperature.

c. Organic spin valves (OSV)

LSMO films grown by PLD are also frequently used as spin injector in organic spintronics, an emerging research field that combines spintronics and molecular/organic electronics. In many of these studies, the LSMO layer contacts an organic semiconductor (OS), which acts as spin transporting medium. The use of

OSs in spintronics is motivated by their long spin relaxation time compared to inorganic materials, which is attributed to weak spin-orbit and hyperfine interactions in light-element compounds. Control over the electronic properties via chemical engineering, low production costs, and ease of large scale fabrication are often used as additional motivation. Several review articles have been published on organic spintronics [107-110]. Here, we only focus on the frequent use of PLD and LSMO in organic spin valves and MTJ devices.

The choice of LSMO in organic spintronics is mainly based on its stability in contact with OS molecules and its high degree of spin polarization. In addition, the work function (≈ 4.9 eV) and low carrier density of LSMO are particularly suitable for efficient spin injection into many organic semiconductors and polymers. In the first report on organic spin valves, Dediu et al. demonstrated a magnetoresistance (MR) effect of 30% at 300 K in a planar geometry with two LSMO electrodes and a 140 nm wide oligomer sexithianyl (T_6) transport channel [111]. A significantly clearer spin-valve response and MR ratio of 40% at 11 K was subsequently obtained in the first vertical spin valve with a LSMO/140 nm Alq_3/Co structure [112]. However, the MR effect, which was attributed to spin-conserved hopping transport in the OS spacer layer, decayed sharply with increasing temperature. In 2006, room-temperature operation of vertical organic spin valves was reported for OS polymer regio-regular poly(3-hexyl thiophene) (RRP3HT) and poly(3-octylthiophene) (P3OT) based devices with a LSMO/RRP3HT/Co [113] and LSMO/P3OT/LSMO [114] structure. In the RRP3HT-based spin valves, the GMR was 80% at 5 K and the effect diminished to 1.5% at room temperature.

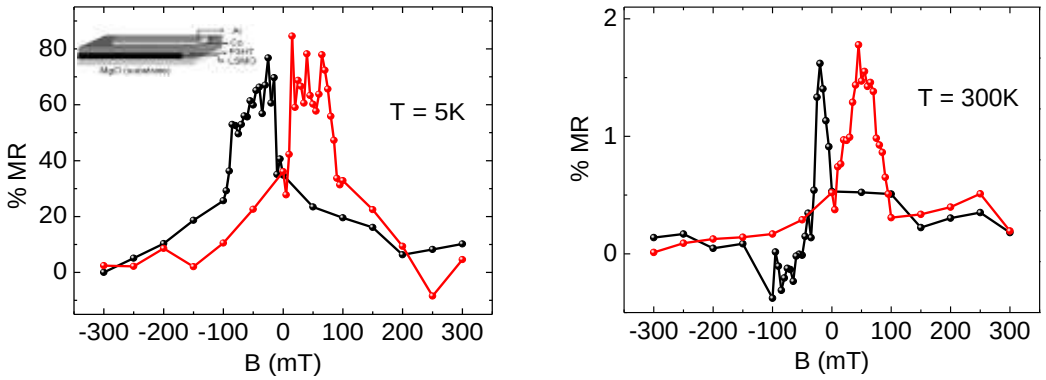

Figure 14. MR response of a LSMO/RRP3HT(100 nm)/Co/Al vertical spin valve at 5K (left) and at room temperature (right). Adapted from Ref. 113 [Majumdar S et al., 2006 *Appl. Phys. Lett.* **89** 122114].

Many studies have been devoted to the physical origin of the strong temperature dependence of MR in organic spin valves [43, 113 - 120]. In one of our efforts, we systematically investigated the influence of the LSMO electrode using PLD on three different substrates (STO, NGO, and MgO) [43]. Not surprisingly, the largest GMR values are obtained for epitaxial LSMO films on STO. However, despite the lower GMR for polycrystalline LSMO on MgO, the temperature variation of the MR effect is very similar on all substrates

(left panel of Fig. 15). This finding suggests that the decrease of GMR signal in organic spin valves at elevated temperatures could be due to deteriorated spin transport in the OS spacer layer. In a later study [119], we particularly focused on polymer RRP3HT-based spin valves with LSMO and Co electrodes. Measurements on these structures indicate that despite nearly constant LSMO spin polarization in the 5 – 50 K temperature range, the MR response is already reduced by half (right panel of Fig. 15). These experimental results suggest that spin-conserved transport through the OS is obtained in the variable-range hopping (VRH) regime (at low temperatures), but that thermally activated polaron hopping destroys the spin information of the carriers at elevated temperatures. Other experiments on the detailed nature of spin scattering mechanisms in OS materials confirm this picture [117, 118, 120].

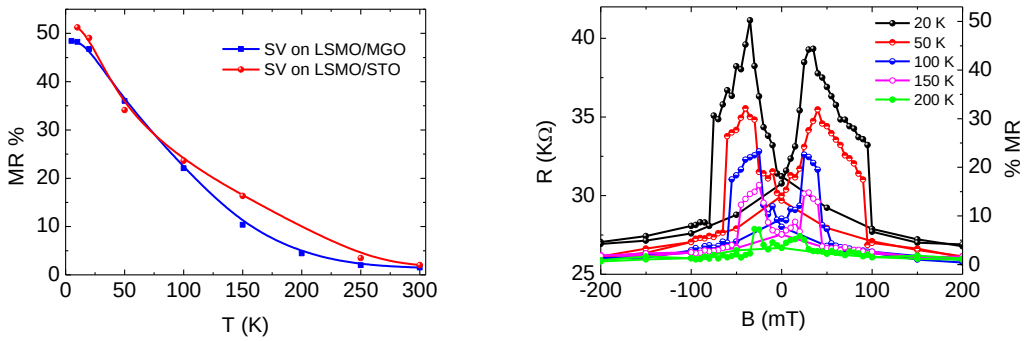

Figure 15. (Left) Temperature dependence of the MR response of a LSMO/RRP3HT/Co spin valve on MgO and STO substrates Adapted from Ref. 42. (Right) GMR response of a LSMO/RRP3HT/Co spin valve on STO at different temperatures. Adapted from Ref. 119 [Majumdar S and Majumdar H S 2012 *Org. Electron.* **13** 2653].

LSMO – OS interfaces: Besides the LSMO electrode and the OS transport channel, properties of the LSMO-OS interface are also crucial for the GMR response of organic spin valves. Several experiments have focused on the electronic and spin injection properties of such interfaces. Engineering of the interface between LSMO and an OS polymer was, for example, investigated using XPS [113]. For a LSMO/RRP3HT interface, a chemical reaction between LSMO and RRP3HT was identified by studying the core level spectra of the Sulphur *2p* peaks, a constituent atom of RRP3HT [113]. Once RRP3HT is coated on LSMO, the pristine LSMO surface disappeared. Cleaning with acetone and alcohol was unable to reduce the sulphur bonding and restore the pristine state of LSMO. The introduction of monolayers of two different organic insulators in the tunneling limit, however, did partially or completely destroy the chemical bonding between RRP3HT and LSMO and this resulted in negligible spin injection. Different devices were studied with varying degrees of chemical bonding between LSMO and RRP3HT and from this it was concluded that spin injection from the ferromagnetic half-metal into the OS decreases systematically when the chemical bond is weakened. Similar chemical reactions between LSMO and organic molecules were also reported in Ref. 121. Later a

photoelectron spectroscopy (PES) study of the interface in LSMO/Alq_3/Co SVs by Zhan et al. [122] revealed the introduction of OS small molecule Alq_3 on LSMO creates a strong interface dipole of 0.9 eV that shifts the energy levels of Alq_3 with respect to the vacuum level. Due to this energy level shift, electron injection into Alq_3 becomes more favorable than hole injection. An unperturbed band diagram favors the injection of holes over the injection of electrons in Alq_3. The dipole moment of the Alq_3 molecule itself was suggested to be the origin of the interface dipole. They also suggested this to be the origin of the inverse sign of magnetoresistance in such devices, which is still a debatable issue.

Interfacial dipole formation of the LSMO/RRP3HT interface is also confirmed by recent magneto-transport experiment [123] and by fitting the transport data with Cheung and Cheung model [124]. This interfacial dipole modifies the barrier height for the injection of spin-polarized carriers from LSMO to the OS layer. For different crystalline qualities of the LSMO film starting from epitaxial on STO to textured on MgO, and finally to completely polycrystalline LSMO on quartz, the application and removal of RRP3HT introduces different GB-like defects in the vicinity of the LSMO surface. The introduction of more GB-like defects leads to a higher resistance and larger LFMR in epitaxial films. However, for the LSMO films on MgO and quartz, with already deteriorated crystalline and transport properties, no significant changes in MR response was found due to the addition or removal of RRP3HT layers. This result signifies that epitaxial thin films of LSMO, considered best for spin injection in polymeric spin valves, undergo degradation at the interface with OSs, extending into bulk regions, by the introduction of GB like defects and carrier localization centers. To achieve better spin injection, different interface engineering between LSMO and OS can be tested. For more details on the organic – ferromagnetic interface including the newly coined “spinterface” science, we refer to review articles on this topic [125, 126].

Besides their usage in organic spin valves, OS materials have also been explored as tunnel barrier in MTJ structures [127-129]. In many experiments, LSMO is used as bottom electrode. While the TMR of organic MTJs can be significant at low temperature (up to 300% at 2 K in Ref. [129]) in nano-junctions, the effect decreases sharply with temperature. Similarly to organic spin valves, the deterioration of TMR at elevated temperatures is attributed to a decrease of interface magnetization in LSMO in combination with enhanced spin scattering during tunneling transport through the OS barrier. Moreover, the TMR of organic MTJs decreases more rapidly with bias voltage than the TMR of inorganic structures. Because of this it is thought that not only magnons, which are known to play a key role in conventional MTJs, but also phonons influence the transport properties of organic junctions.

6. Conclusions and future research

Ferromagnetic half-metallic LSMO thin films have been utilized in experimental studies on spintronics for nearly two decades. During this period, several milestones have been achieved. First, the growth of LSMO thin films and its dependence of PLD growth parameters are now well understood. Second, their integration into spintronics structures has contributed to a better understanding of spin-polarized transport effects, particularly at low temperatures. In the future, LSMO will remain an important material for investigations on fundamental magnetic and electronic transport phenomena. Moreover, its instrumental use in multiferroic tunnel junctions opens up promising possibilities for commercial applications in future nanoelectronics devices. Without the development of PLD 25 years ago, the tremendous advances in complex magnetic oxides and their contribution to the spintronics research field would not have been possible. The engineering of new material properties at the atomic scale is more relevant than ever and, hence, PLD of complex interface is anticipated to unveil more interesting new physics in the future.

Acknowledgements

S M acknowledges financial support from Jenny and Antti Wihuri Founation.

Reference:

[1] Wolf S A, Awschalom D D, Buhrman R A, Daughton J M, von Molnar S, Roukes M L, Chtchelkanova A Y and Treger D M 2001 *Science* **294** 1488

[2] Žutić I, Fabian J and Das Sarma S 2004 *Rev. Mod. Phys.* **76** 323

[3] Baibich M N, Broto J M, Fert A, et al. 1988 *Phys. Rev. Lett.* **61** 2472

[4] Moodera J S, Kinder L R, Wong T M and Meservey R 1995 *Phys. Rev. Lett.* **74** 3273

[5] Tsymbal E Y and Kohlstedt H 2006 *Science* **313** 181

[6] Park J -H, Vescovo E, Kim H -J, Kwon C, Ramesh R and Venkatesan T 1998 *Nature (London)* **392** 794

[7] *Pulsed Laser Deposition of Thin Films*, 1994 ed. Chrisey D B and Hubler G K (Wiley VCH) ISBN 0-471-59218-8, p. 648

[8] Dagotto A, Hotta T and Moreo A 2001 *Phys. Rep.* **344** 1

[9] Cesaria M, Caricato A P, Maruccio G and Martino M 2011 *Journal of Physics: Conference Series* **292** 012003

[10] Zhang M, Ma X L, Li D X, Lü H B, Chen Z H and Yang G Z 2003 *Phys. Stat. Sol. (a)* **196** 365

[11] Meservey R and Tedrow PM 1994 *Phys. Rep.* **238** 173

[12] Monsma D J and Parkin S S P 2000 *Appl. Phys. Lett.* **77** 720

[13] Kaiser C, van Dijken S, Yang S -H, Yang H and Parkin S S P 2005 *Phys. Rev. Lett.* **94** 247203

[14] Ranno L, Llobet A, Hunt M B and Pierre J 1999 *Appl. Surf. Sci.* **138–139** 228

[15] Fujishiro H, Fukase T and Ikebe M, 1998 *J. Phys. Soc. Jpn.* **67** 2582

[16] Zener C 1951 *Phys. Rev.* **82** 403

[17] Jonker G H and Van Santen J H 1950 *Physica (Amsterdam)* **16** 337

[18] Anderson P W and Hasegawa H 1955 *Phys. Rev.* **100** 675

[19] Ramirez A P 1997 J. Phys.: Condens. Matter 9 8171

[20] Millis A J, Shraiman B I and Mueller R 1996 *Phys. Rev. Lett.* 77 175

[21] Millis A J, Littlewood P H and Shraiman B I 1995 *Phys. Rev. Lett.* 74 5144

[22] Millis A J 1998 *Nature* 392 147

[23] Sun J Z and Gupta A 1998 *Annu. Rev. Mater. Sci.* **28** 45

[24] Muduli P K, Singh G, Sharma R and Budhani R C 2009 *J. Appl. Phys.* **105** 113910

[25] Urushibara A, Moritomo Y, Arima T, Asamitsu A, Kido G and Tokura Y 1995 *Phys. Rev. B* **51** 14103

[26] Jeffrey Snyder G, Hiskes R, Dicarolis S, Beasley M R and Geballe T H 1996 *Phys. Rev. B* **53** 14434

[27] Sun J Z, Abraham D W, Rao R A and Eom C B 1999 *Appl. Phys. Lett.* **74** 3017

[28] Li J, Ong C K, Liu J M, Huang Q and Wang S J 2000 *Appl. Phys. Lett.* **76** 1051

[29] Rajeswari M, Shreekala R, Goyal A, Lofland S E, Bhagat S M, Ghosh K, Sharma R P, Greene R L, Ramesh R, Venkatesan T and Boettcher T 1998 *Appl. Phys. Lett.* **73** 2672

[30] Kwon C, Robson M C, Kim K-C, Gu J Y, Lofland S E, Bhagat S M, Trajanovic Z, Rajeswari M, Venkatesan T, Kratz A R, Gomez R D and Ramesh R 1997 *J. Magn. Magn. Mater*. **172** 229

[31] Desfeux R, Bailleul S, Da Costa A, Prellier W and Haghiri-Gosnet A M 2001 *Appl Phys Lett.* **78** 3681

[32] S Y Yang, W L Kuang, Y Liou, W S Tse, S F Lee and Y D Yao 2004 *J. Magn. Magn. Mater*. **268** 326

[33] Haghiri-Gosnet A -M and Renard J -P 2003 *J. Phys. D: Appl. Phys.* **36** R127

[34] Liu J-M, Zhang Y X, Liu Z G, Du Y W, Zhang H H, Yu Z and Ong C K 2002 *J Phys.: Condens. Mat.* **14** 3167

[35] Joonghoe D, Hur N H, Kim I S and Park Y K 2003 *J. Appl. Phys.* **94** 7670

[36] Kawasaki M, Izumi M, Konishi Y, Manako T and Tokura Y 1999 *Mater. Sc. and Eng. B* **63** 49

[37] Malavasi L, Mozzati M C, Azzoni C B, Tealdi C and Flor G 2006 *J. Magn. Magn. Mater*. **310** e193

[38] Meda L, Kennon L, Bacaltchuk C, Garmestani H and Dahmen K H 2001 *J. Mater. Res.* **16** 1887

[39] Suzuki Y, Hwang H Y, Cheong S W, Siegrist T, van Dover R B, Asamitsu A and Tokura Y 1998 *J. Appl. Phys*. **83** 7064

[40] Wu J Y, Suzuki Y, Rudiger U, Yu, Kent A D, Nath T K and Eom C B 1999 *Appl. Phys. Lett.* **75** 2295

[41] Majumdar S, Huhtinen H, Majumdar H S, and Paturi P 2012 *J. Alloys and Compounds* **512** 332

[42] Majumdar S, Huhtinen H, Paturi P and Majumdar H S 2013 *J. Mater. Sci.* **48** 2115

[43] Majumdar S, Huhtinen H, Majumdar H S, Laiho R, and R. Österbacka 2008 *J. Appl. Phys.* **104** 033910

[44] Garcia V, Bibes M, Barth´el´emy A, Bowen M, Jacquet E, Contour J -P and Fert A 2004 *Phys. Rev. B* **69** 052403

[45] Kavich J J, Warusawithana M P, Freeland J W, Ryan P, Zhai X, Kodama R H and Eckstein J N 2007 *Phys. Rev. B* **76** 014410

[46] Freeland J W, Kavich J J, Gray K E, Ozyuzer L, Zheng H, Mitchell J F, Warusawithana M P, Ryan P, Zhai X, Kodama R H and Eckstein J N 2007 *J. Phys.: Cond. Mat.* **19** 315210

[47] Harrison W A, Kraut E A, Waldrop J R and Grant R W 1978 *Phys. Rev. B* **18** 4402

[48] Baraff G A, Appelbaum J A and Hamann D R 1977 *Phys. Rev. Lett.* **38** 237

[49] Yamada H, Ogawa Y, Ishii Y, Sato H, Kawasaki M, Akoh H and Tokura Y 2004 *Science* **305** 646

[50] Ishii Y, Yamada H, Sato H, Akoh H, Ogawa Y, Kawasaki M and Tokura Y 2006 *Appl. Phys. Lett.* **89** 042509

[51] Majumdar S, Kooser K, Elovaara T, Huhtinen H, Granroth S and Paturi P 2013 *J. Phys.: Condens Mat.* **25** 376003

[52] Julliere M 1975 *Phys. Lett.* **54A** 225

[53] Kim E J, Watts J L R, Harteneck B, Scholl A, Young A, Doran A and Suzuki Y 2011 *J. Appl. Phys.* **109** 07D712

[54] Bibes M and Barth´el´emy A 2007 *IEEE Trans. Electron. Dev.* **54** 1003

[55] Lu Y, Li W, Gong G, Xiao G, Gupta A, Lecoeur P, Sun J, Wang Y and Dravid V 1996 *Phys. Rev. B* **54** R8357

[56] Sun J Z, Gallagher W J, Ducombe P R, Krusin-Elbaum L, Altman R A, Gupta A, Lu Y, Gong G Q and Xiao G 1996 *Appl. Phys. Lett.* **69** 3266

[57] Bowen M, Bibes M, Barthélémy A, Contour J -P, Anane A, Lemaˆıtre Y and Fert A 2003 *Appl. Phys. Lett.* **82** 233

[58] Jo M-H, Mathur N D, Evetts J E and Blamire M G 2000 *Appl. Phys. Lett.* **77** 3803

[59] Lu Y, Li X W, Gong G Q, Xiao G, Gupta A, Lecoeur P, Sun J Z, Wang Y Y and Dravid V P 1996 *Phys. Rev. B* **54** R8357

[60] Viret M, Drouet M, Nassar J, Contour J -P, Fermon C and Fert A 1997 *Europhys. Lett.* **39** 545

[61] Obata T, Manako T, Shimakawa Y and Kubo Y 1999 *Appl. Phys. Lett.* **74** 290

[62] Jo M –H, Mathur N D, Todd N K and Blamire M G 2000 *Phys. Rev. B* **61** R14905

[63] Sun J Z, Krusin-Elbaum L, Duncombe P R, Gupta A and Laibowitz R B 1997 *Appl. Phys. Lett.* **70** 1769

[64] Sun J 1998 *Phil. Trans. R. Soc. London A* **356** 1693

[65] Bowen M, Barth´el´emy A, Bibes M, Jacquet E, Contour J-P, Fert A, Ciccacci F, D`uo L and Bertacco R 2005 *Phys. Rev. Lett.* **95** 137203

[66] Gu R Y, Sheng L and Ting C S 2001 *Phys. Rev. B* **63** 220406(R)

[67] Bertacco R, Portalupi M, Marcon M, D`uo L, Ciccacci F, Bowen M, Contour J -P and Barth´el´emy A 2002 *J. Magn. Magn. Mater.* **242** 710

[68] Muduli P K and Budhani R C 2009 *J. Appl. Phys.* **106** 103924

[69] Bowen M et al. 2007 *J. Phys.: Condens. Matter* **19** 315208

[70] De Teresa J M, Barthélémy A, Fert A, Contour J -P, Montaigne F and Seneor P 1999 *Science* **286** 507

[71] Hayakawa J, Kokado S, Ito K, Sugiyama M, Asano H, Matsui M, Sakuma A and Ichimura M 2002 *Jpn. J. Appl. Phys.* **41** 1340

[72] Hayakawa J, Ito K, Kokado S, Ichimura M, Sakuma A, Sugiyama M, Asano H and Matsui M 2002 *J. Appl. Phys.* **91** 8792

[73] Rizwan S, Guo S M, Wang Y et al. 2010 *IEEE Trans. Magn.* **46** 2383

[74] Fert A, Barthélémy A, Ben Youssef J, Contour J -P, Cros V, De Teresa J M et al. 2001 *Mat. Sc. Eng. B* **84** 1

[75] Kumigashira H, Chikamatsu A, Hashimoto R, Oshima M, Ohnishi T, Lippmaa M, Wadati H, Fujimori A, Ono K, Kawasaki M and Koinuma H 2006 *Appl. Phys. Lett.* **88** 192504

[76] Yamada H, Ogawa Y, Ishii Y, Sato H, Kawasaki M, Akoh H, Y Tokura 2004 *Science* **305** 646

[77] Ishii Y, Yamada H, Sato H, Akoh H, Ogawa Y, Kawasaki M and Tokura Y 2006 *Appl. Phys. Lett.* **89** 042509

[78] Kautz J 2009 *Master Thesis*, University of Twente and references therein (http://www.utwente.nl/tnw/ims/people/formerMSc/Jaap%20Kautz.pdf)

[79] Ma J, Hu J, Li Z, Nan C -W 2011 *Adv. Mater.* **23** 1062

[80] Vaz C A 2012 *J. Phys.: Condens. Mat.* **24** 333201

[81] Thiele C, Dörr K, Fähler S, Schultz L, Meyer D C, Levin A A and Paufler P 2005 *Appl. Phys. Lett.* **87** 262502

[82] Thiele C, Dörr K, Bilani O, Rödel J and Schultz L 2007 *Phys. Rev. B* **75** 054408

[83] Zheng R K, Wang Y, Chan H L W, Choy C L and Luo H S 2007 *Phys. Rev. B* **75** 212102

[84] Wang J, Hu F X, Li R W, Sun J R, and Shen B G 2010 *Appl. Phys. Lett.* **96** 052501

[85] Kim J -Y, Lide Y and van Dijken S 2013 *J. Phys.: Condens. Mat.* **25** 082205

[86] Gajek M, Bibes M, Fusil S, Bouzehouane K, Fontcuberta J, Barthélémy A and Fert A 2007 *Nature Mater.* **6** 296; Béa H, Bibes M, Cherifi S et al. 2006 *Appl. Phys. Lett.* **89** 242114

[87] Garcia V, Fusil S, Bouzehouane K, Enouz-Vedrenne S, Mathur N D, Barthélémy A and Bibes M 2009 *Nature* **81** 460

[88] Chanthbouala A, Crassous A, Garcia V et al. 2012 *Nature Nanotech.* **7** 101

[89] Yin Y W, Burton J D, Kim Y -M et al. 2013 *Nature Mater.* **12** 397

[90] Wen Z, Li C, Wu D, Li A and Ming N 2013 *Nature Mater.* **12** 617

[91] Tsymbal E Y and Kohlstedt H 2006 *Science* **313** 181

[92] Zhuravlev M Ye, Sabirianov R F, Jaswal S S, and Tsymbal E Y 2005 *Phys. Rev. Lett.* **94** 246802

[93] Kohlstedt H, Pertsev N A, Rodríguez Contreras J and Waser R 2005 *Phys. Rev. B* **72** 125341

[94] Ikeda S, Hayakawa J, Ashizawa Y et al. 2008 *Appl. Phys. Lett.* **93** 082508

[95] Maksymovych P, Jesse S, Yu P, Ramesh R, Baddorf A P and Kalinin S V 2009 *Science* **324** 1421

[96] Gruverman A, Wu D, Lu H, Wang Y, Jang H W, Folkman C M, Zhuravlev M Ye, Felker D, Rzchowski M, Eom C -B and Tsymbal E Y 2009 *Nano Lett.* **9** 3539

[97] Pantel D, Goetze S, Hesse D and Alexe M 2011 *ACS Nano* **5** 6032

[98] Garcia V, Bibes M, Bocher L, Valencia S, Kronast F, Crassous A., Moya X, Enouz-Vedrenne S, Gloter A, Imhoff D, Deranlot C, Mathur N D, Fusil S, Bouzehouane K and Barthélémy A 2010 *Science* **327** 1106

[99] Valencia S, Crassous A, Bocher L et al. 2011 *Nature Mater.* **10** 753

[100] Pantel D, Goetze S, Hesse D and Alexe M 2012 *Nature Mater.* **11** 289

[101] Duan C -G, Jaswal S S and Tsymbal E Y 2006 *Phys. Rev. Lett.* **97** 047201

[102] Burton J D and Tsymbal E Y 2011 *Phys. Rev. Lett.* **106** 157203

[103] Hong X, Posadas A, Lin A, and Ahn C H 2003 *Phys. Rev. B* **68** 134415

[104] Molegraaf H J A, Hoffman J, Vaz C A F, Gariglio S, van der Marel D, Ahn C H and Triscone J -M 2009 *Adv. Mater.* **21** 3470

[105] Vaz C A F, Hoffman J, Segal Y, Reiner J W, Grober R D, Zhang Z, Ahn C H and Walker F J 2010 *Phys. Rev. Lett.* **104** 127202

[106] Lu H, George T A, Wang Y et al. 2012 *Appl. Phys. Lett.* **100** 232904

[107] Naber W J M, Faez S, and van der Wiel W G 2007 *J Phys. D: Appl. Phys.* **40** R205

[108] Dediu V A, Hueso L E, Bergenti I and Taliani C 2009 *Nat. Mater.* **8** 707

[109] Majumdar S, Majumdar H S and Österbacka R 2011 *Comprehensive Nanoscience and Technology* vol. 1 (Oxford Academic Press) p. 109

[110] Alam K M and Pramanik S 2011 *Nano-Semiconductors: Devices and Technology* (CRC press) p. 87

[111] Dediu V A, Murgia M, Matacotta FC, Taliani C, and Barbanera S 2002 *Solid State Communication* **122** 181

[112] Xiong Z H, Wu D, Valy Vardeny Z and Shi J 2004 *Nature (London)* **427** 821

[113] Majumdar S, Laiho R, Laukkanen P, Väyrynen I J, Majumdar H S, and Österbacka R 2006 *Appl. Phys. Lett.* **89** 122114

[114] Kumar J, Singh R K, Siwach P K, Singh H K, Singh R, Rastogi R C and Srivastava O N 2006 *Solid State Comm.* **138** 422

[115] Dediu V, Hueso L E, Bergenth I, et al. 2008 *Phys. Rev. B* **78** 115203

[116] Wang F J, Yang C G and Valy Vardeny Z 2007 *Phys. Rev. B* **75** 245324

[117] Drew A, Hoppler J, Schulz L et al. 2009 *Nature Mater.* **8** 109

[118] Bandopadhyay S 2010 *Phys. Rev. B* **81** 153202

[119] Majumdar S and Majumdar H S 2012 *Org. Electron.* **13** 2653

[120] Majumdar S and Majumdar H S 2013 *Synth. Met.* **173** 26

[121] Grobosch M, Dorr K, Gangineni R B and Knupfer M 2009 *Adv. Eng. Mater.* **11** 285

[122] Zhan Y, Bergenti I, Hueso LE, Dediu V, de Jong MP, and Li ZS 2007 *Phys. Rev. B* **76** 045406

[123] Pesonen M, Majumdar S, Huhtinen H, Paturi P, Majumdar H S and Österbacka R 2013 *AIP Adv* **3** 042102

[124] Cheung S K and Cheung N W 1986 *Appl. Phys. Lett.* **49** 85

[125] Zhan and Fahlman 2012 *J. Pol. Sc. B: Pol. Phys.* **50** 1453

[126] Grobosch M and Knupfer M 2010 *The Open Appl. Phys. Journal* **4** 8

[127] Santos T S, Lee J S, Migdal P, Lekshmi I C, Satpati B and Moodera J S 2007 *Phys. Rev. Lett.* **98** 016601

[128] Yoo J –W, Chen C –Y, Jang H W, Bark C W, Prigodin V N, Eom C B, Epstein A J 2010 *Nature Mat.* **9** 638

[129] Barraud C, Seneor P, Mattana R et al., 2010 *Nature Phys.* **6** 615